JOINT RESAMPLING AND RESTORATION OF HEXAGONALLY SAMPLED IMAGES USING ADAPTIVE WIENER FILTER

Thesis

Submitted to

The School of Engineering of the

UNIVERSITY OF DAYTON

In Partial Fulfillment of the Requirements for

The Degree of

Master of Science in Electrical Engineering

By

Ranga Burada

UNIVERSITY OF DAYTON

Dayton, Ohio

December, 2015

JOINT RESAMPLING AND RESTORATION OF HEXAGONALLY SAMPLED IMAGES USING ADAPTIVE WIENER FILTER

Name: Burada, Ranga

APPROVED BY:

Russell C. Hardie, Ph.D. Advisory Committee Chairman Professor Electrical and Computer Engineering	John S. Loomis, Ph.D. Committee Member Professor Electrical and Computer Engineering

Guru Subramanyam, Ph.D.
Committee Member
Professor
Electrical and Computer Engineering

John G. Weber, Ph.D. Associate Dean School of Engineering	Eddy M. Rojas, Ph.D.,M.A.,P.E. Dean School of Engineering

ABSTRACT

JOINT RESAMPLING AND RESTORATION OF HEXAGONALLY SAMPLED IMAGES USING ADAPTIVE WIENER FILTER

Name: Burada, Ranga
University of Dayton

Advisor: Dr. Russell C. Hardie

The premier objective of this research is to study the non-uniform interpolation to resample a hexagonally sampled image to a regular rectangular grid and to show hexagonal sampled data is more efficient than rectangular sampled data using an Adaptive Wiener Filter (AWF).

Image processing is very important in several applications and have been using in them very efficiently. Digital image acquisition hardware, such as digital cameras, take photos by recording images as digital data using optics and a detector array. Distortions such as blur, noise and aliasing are often present, and these degrade image quality. For such reasons, image restoration algorithms are often applied to acquired images to reduce the degradations. Normally we use a rectangular sampling to digitize a continuous scene. There could be some other approaches to use as an alternate for this. One approach is to change the sampling process from rectangular pattern to hexagonal sampling pattern, considering various advantages. There is no inconsis-

tency in pixel connectivity and thus angular resolution is higher in this arrangement and also fewer less samples need to represent the data represented in rectangular pattern. This research gives an overview of implementation of hexagonal sampling can be done by simulating a hexagonal sampled camera and adapt AWF to hexagonal sampling. Apply new AWF to simulated data quantitatively and qualitatively evaluate performance verses a standard rectangular sampling camera.

ACKNOWLEDGMENTS

Though the following thesis is an individual work, I could never have reached the heights or explored the depth with out the help, support, guidance and efforts of lot of people. Firstly, I would like to thank my parents for their continuing support.

I would like to take this opportunity to thank Dr. Russell Hardie for all his support and guide me through graduate school. I have learned good knowledge and gained practical experience while doing course work and thesis under him.

I would like to thank Dr. Guru Subramanyam and entire Elecetical Engineering Department for supporting my thesis and for providing a chance to work as a Graduate Assistant.

I would like to thank Dr. Khaled Mohamed for supporting me through out my entire thesis. He gave lot of suggestions and clarified so many questions from base level. One of the most important person in my master's journey.

I have used Adaptive weiner Filter block diagram and would like to acknowledge Dr. Russell Haride for his support in this.

A very special thank you to my friends for their support they've lent me over the years. Thanks a lot for everything.

I would to thank my committee for taking time out of their schedules to review my thesis and be part of my defense.

Finally, I would like to mention one more thing i.e my Internship experience. I would like to thank Dr. Russell Hardie for allowing me to work for 6 months as a Intern at ON Semiconductor. I have learned great productive things from my Internship.

TABLE OF CONTENTS

LIST OF FIGURES

LIST OF TABLES

CHAPTER 1

INTRODUCTION

1.1 Object of the Study

Taking images are important in many aspects in life, medically and geographically. No matter which sampling scheme is chosen, an insufficient sampling rate can always lead to undesirable effects in the reconstructed signal, known as aliasing. Over the past years the researchers have been studying the advantages of hexagonal grid in the area of image processing and published more details on this topic. There are several grid patters available to represent the digitized image, normally continuous scenes are sampled and displayed on a square grid pattern and here we are changing the square grid pattern to hexagonal grid pattern for hexagonal image processing. Because of it's various advantages over the later. Out of many advantages for the hexagonal structure in image processing, the primary one is it's higher degree of circular symmetry, uniform connectivity, greater angular resolution[9] and in some applications hexagonal sampling [12] is a promising solution with better efficiency and less aliasing.

Hexagonal grid patterns are more attractive than the regular rectangular because they exploit the oblique effect in human vision which makes us less sensitive to the edges in the diagonal rather than horizontal or vertical directions[11]. At the present

time, the combination of hexagonal sampling and a device which has a hexagonal grid pattern is very difficult to find but there are ways to simulate a hexagonal grid on a regular rectangular grid device to display the hexagonally sampled scene.

1.2 Re-sampling

Re-sampling is the process of transforming a discrete image which is defined at one set of coordinate locations to a new set of coordinate points i.e converting from rectangular to hexagonal grid. Using alternative shapes for pixels can also address the problem of curve representation. Hexagonal shaped pixels are attractive since they exploit the oblique effect in human vision which makes us less sensitivity to the edges in the diagonal rather than horizontal or vertical directions. This results in better performance when representing curved shapes. This whole idea is possible when we re-sample the the square grid to the hexagonal grid pattern. Aliasing is the other issue that we can overcome with the help of this pattern.

1.3 Significance of the Study

In this research we present a computationally efficient re-sample and restoration algorithm to address sampling and aliasing for the Nyquist sampled imaging system. The proposed method utilizes an hexagonal sampling technique followed by an adaptive wiener filter (AWF)[2]. At the present time, a real hexagonal grid device is very difficult to find. Fortunately, there are ways to simulate a hexagonal grid on a regular square grid device[3]. There are two stages in this study. Re-sampling is the initial

stage to sample the image and restoration is the other techniques, where we estimate the high resolution grid from the hexagonal sampled grid. The restoration process is done by the AWF.

Amoung all the researcher, Peterson and Middleton [10] addressed the general sampling scheme in 2-D images and in their method they showed the hexagonal grid was optimal for circularly band limited scenes and 13.4% fewer samples required compared to rectangular sampling, Mersereau[8] investigated theories concentrating on the processing of hexagonally sampled 2-D signals. The hexagonal grid pattern can form by combining two rectangular sampling grids and this process is suggested by Luczak and Rosenfeld [7] in name of pseudohexagonal grid.

At present,the resampling theories and interpolation schemes on the traditional rectangular grids are already well developed and presented[6], Golay [1], an early pioneer of hexagonal grid studies, was the first researcher to bring to public attention the distinct advantages of this grid type. Continuing the Mersereau[8] work, Dubois extended the sampling and reconstruction theory to three-dimensionally sampled video signals on various non-square lattices. More recently, Wuthrich and Stucki[14] tried to simulate a hexagonal grid on a high resolution rectangular device for computer graphics utilization. Her [4] invented a unique coordinate system to be used on the hexagonal grids, and based on this coordinate frame, he also studied various geometrical transformations on hexagonal grids.

Under sampling is a process in which samples with continuous signals below the nyquist rate of images is a huge problem that causes aliasing and loosing data. To overcome this problem we implement super resolution (SR) with hexagonal sampling

using a proven method of Adaptive Wiener Filter (AWF) SR[2] to produce High Resolution (HR) image without any aliasing. Adaptive Wiener filter is a popular method to produce a HR image using multi frame input. This method works based on sliding window to calculate weights for each and every HR pixel. Considering this method for this proposed research, we take the advantage of non-uniform interpolation to get the uniform pattern from non-uniform pixel tessellation. The purpose of this paper is to investigate the hexagonal sampling and its advantages. This research contains two main stages, one is rectangular to hexagonal re-sampling and the other is hexagonal to rectangle re-sampling.

1.4 Organization of the Thesis

The remaining thesis is organized as follows. Section 2 describes the observation model and the type of sampling scheme used. The resampling and restoration scheme is presented in section 3. Experimental results are provided in section 4 and finally, conclusions are presented in section 5.

CHAPTER 2

OBSERVATION MODEL

In this section we discuss the observation model that describes the forward process of forming the low resolution image from a continuous scene $d(x, y)$, where x,y are the are continuous spatial coordinate and how they are related to the ideal High Resolution (HR) image is shown in Fig.1. This is a single frame version of the model used in Adaptive Wiener Filter Super Resolution (AWF SR)[2]. The AWF SR algorithm takes multiple LR frames to form a single HR image but in this propose research we consider single low resolution (LR) image to estimate high resolution (HR) image so there is no motion estimation is considered. The image is convolved with system point spread function (PSF) and we address the Optical transfer function and spatial sampling in details in Chapter 2.1 and 2.2 respectively and then packing of the detectors are discussed in chapter 2.3.

2.1 Optical Transfer Function

The PSF is designed to include the diffraction and detector integration. In the proposed research we consider two different detectors, regular rectangular and hexagonal detector. the continuous image, *d(x,y)* is covolved with PSF, *h(x,y)* yields the

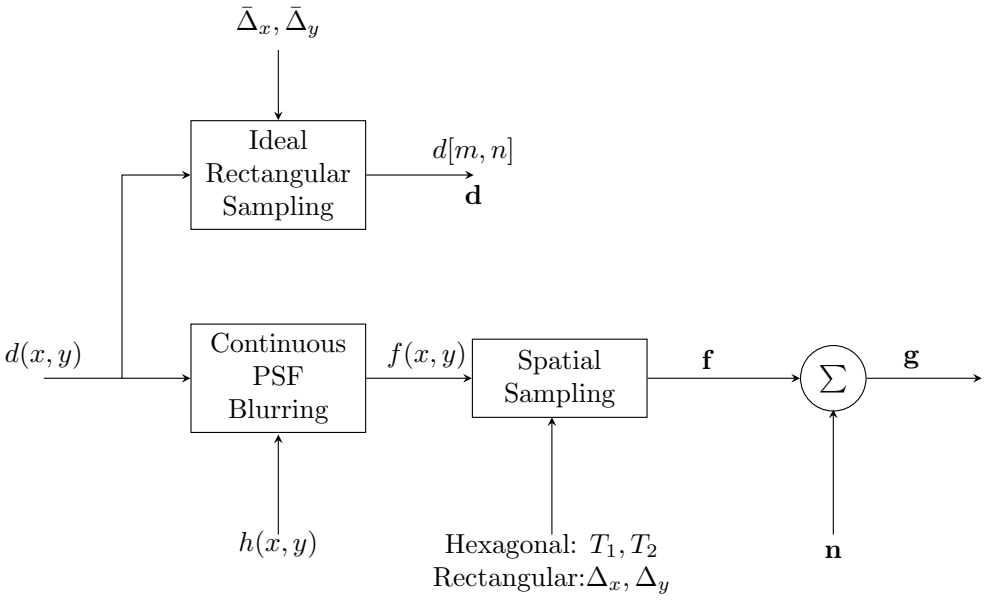

Figure 2.1: Single Frame Continuous Input (physical acquisition system).

intermediate image *f(x,y)*, is show in eq.1.

$$f(x,y) = d(x,y) * h(x,y) \tag{2.1}$$

where *f(x,y)* is the noise free version of *d(x,y)* and *h(x,y)*. To model the PSF, that models diffraction and detector integration. The diffraction of both the detectors are same but detector limitations are different.

$$h(x,y) = F^{-1}\{H(u,v)\}, \tag{2.2}$$

where

$$H(u,v) = H_{det}(x,y).H_{dif}(x,y) \tag{2.3}$$

where $H(u,v)$ is the continuous frequency of the PSF. The rectangular detectors with the dimensions of Δ_x in x-direction and Δ_y in y-direction. The shape of the detector is shown in Fig .2.2a, and the detector PSF would be given by

$$h_{rect}(x,y) = \frac{1}{ab} rect(\frac{x}{a}, \frac{y}{b}) = \begin{cases} 1 & \text{if } \left|\frac{x}{a}\right| < \frac{1}{2} \ \& \ \left|\frac{x}{b}\right| < \frac{1}{2} \\ 0 & \text{otherwise} \end{cases} \tag{2.4}$$

where a and b are the physical dimensions of the active area of a single detector measured in micrometers (μm).As a result, the Optical Transfer Function (OTF) of such detector array can be defined as

$$H_{det}(u,v) = \text{sinc}(au)\text{sinc}(bv) = (\frac{\sin(\pi au)}{au})(\frac{\sin(\pi bv)}{bv}), \tag{2.5}$$

where u,v are the frequencies in horizontal and vertical directions, respectively measured in cycle/μm.

The other type of detector is Hexagonal detector shown in Fig .2.2b with the dimensions of T1 in x-direction and T2 in y-direction. In this case we don't have a physical formula to represent but the Fast Fourier Transform of the Hexagonal shape is shown in Fig .2.2d.

As we mentioned earlier the diffraction of both the detectors are same and the

OTF of the diffraction of the optics with the circular exit pupil can be expressed as

$$H_{dif}(u,v) = \begin{cases} \frac{2}{\pi}[\cos^{-1}(\frac{\rho}{\rho_c}) - \frac{\rho}{\rho_c}\sqrt{1-(\frac{\rho}{\rho_c})^2} & \text{if } \rho < \rho_c \\ 0 & \text{otherwise} \end{cases} \tag{2.6}$$

where $\rho = \sqrt{u^2+v^2}$ is the radial frequency of the OTF,and the ρ_c is radial cutoff frequency. ρ_c is given by

$$\rho_c = \frac{1}{\lambda f/\#} \tag{2.7}$$

Where λ is the wavelength of light and $f/\#$ is defined as the ratio of the focal length to the effective diameter of the optics. Another important parameter is the detector pitch is shown in Fig. 2.3 as Δ_x and Δ_y for the focal plane array. The pitch is the spacing between the detector elements and it controls the sampling frequency. The sampling frequency in x and y directions are $\frac{1}{\Delta_x}$ and $\frac{1}{\Delta_y}$, respectively. According to The Nyquist criterion, is important to avoid the aliasing and we must satisfy below equation

$$\delta_s \leq \frac{1}{2\rho_c} = \frac{\lambda f/\#}{2}. \tag{2.8}$$

However, due to the complex structure in imaging systems design, many imaging systems do not meet the Nyquist criterion. The Impulse invariant Discrete frequency responses are shown in Fig. 2.c, Fig. 2.d for rectangular and hexagonal detectors respectively. The combined detector and diffraction blur of both the detectors are shown in Fig. 2.e and Fig. 2.f respectively.

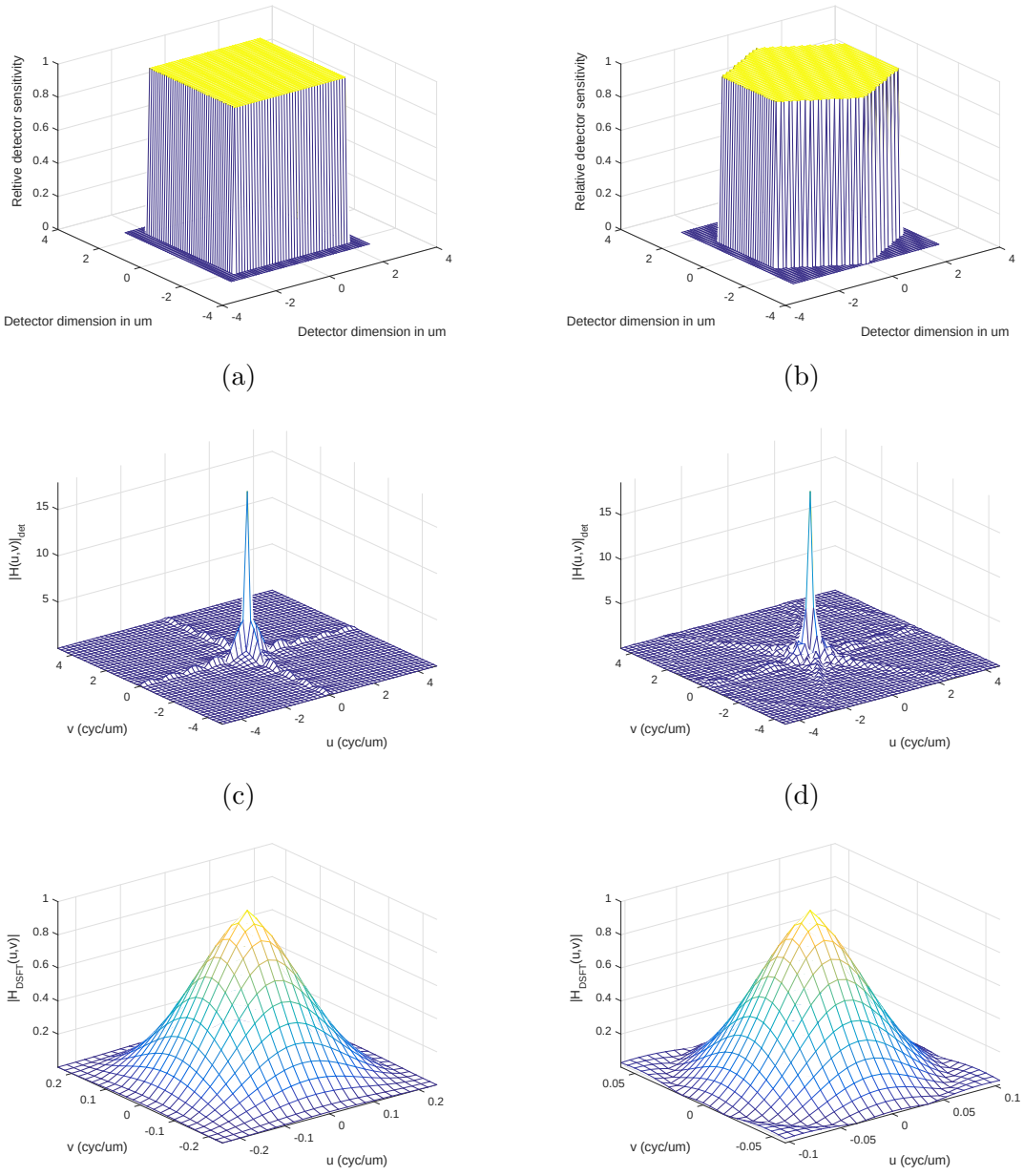

Figure 2.2: (a)Rectangular Detector shape (b) Hexagonal Detector shape when, $pitch = 2\mu m$, $\lambda = 0.5\mu m$, $f - num = 4$. (c) Rectangular detector blur when, $pitch = 2\mu m$, (d) Hexagonal Detector blur when, $pitch = 1\mu m$, with $\lambda = 0.5\mu m$, $f - num = 4$. Detector and Diffraction blur for (e) Rectangular. (f) Hexagonal.

2.2 Spatial Sampling

In order to become suitable for digital processing, an image must be digitized both spatially and in amplitude. Hence in order to create an image which is digital, we need to convert continuous data into digital form. There are two ways in which it is done. Rectangular sampling and followed by hexagonal sampling are discussed in Chapter 2.2.1 and 2.2.2.

2.2.1 Rectangular Sampling

The rectangular sampling [13] is a common sampling scheme performed in all cameras. The output from the PSF is an intermediate continuous scene,*f(x,y)*, is sampled rectangularly based on the motion paramenters and the dectecor pitch of the (FPA) as desccribed in [4] with the detector pitch is shown in Fig. 1 as Δ_x and Δ_y. These samples are represented in lexicographical notation as $f = [f_1, f_2, ...f_N]^T$ and the distribution of the pixels are shown in Fig. 2.3., where Δ_x is in horizontal direction and Δ_y is in vertical direction.

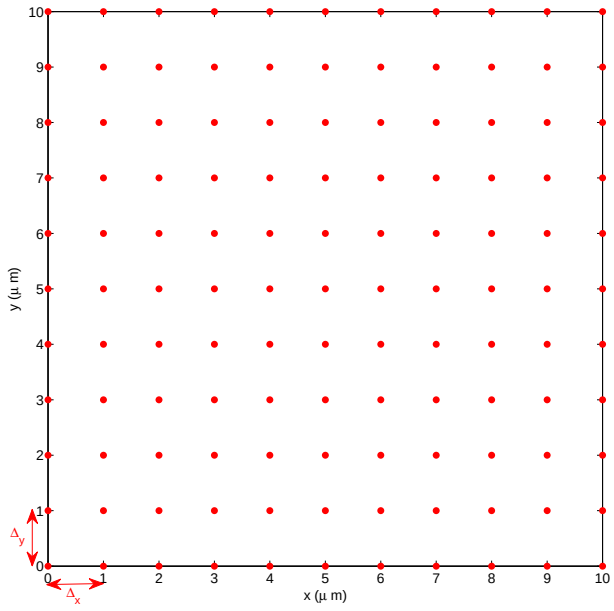

Figure 2.3: Rectangular Sampling grid for $\Delta_x = \Delta_y = 1\ \mu m$.

2.2.2 Hexagonal Sampling

However, in practice the commonly available sampling lattice is rectangular lattice, know as rectangular sampling. But taking the advantage of hexagonal pattern we consider the other type of detector layout is hexagonal detector. To generate hexagonal detector [13] the detector pitch is choosen as Δ_{T_1} and Δ_{T_2}. There are two possible ways to generate a hexagonal lattice, one with the regular hexagonal co-ordinates and other one taking the advantage of the repeating patterns after some samples. We choose the pseudo hexagonal coordinates [3], for better performance in terms of simulation [12]. The distribution of the hexagonal pattern is shown in Fig. 2.4., where $LT1$ is in horizontal direction and $LT2$ is in Vertical direction and L is downsampling factor. For user convenience the hexagonal co-ordinates are,

$H_1 = \{(1,0),(\frac{1}{2},\frac{\sqrt{3}}{2})\}$, $H_2 = \{(\frac{\sqrt{3}}{2},\frac{1}{2}),(0,1),\}$. In particular the hexagonal sampling parameters are $\Delta_{T_1} = \frac{2}{\sqrt{3}}$ and $\Delta_{T_2} = 2$ considered in this proposed hexagonal sampling AWF SR.

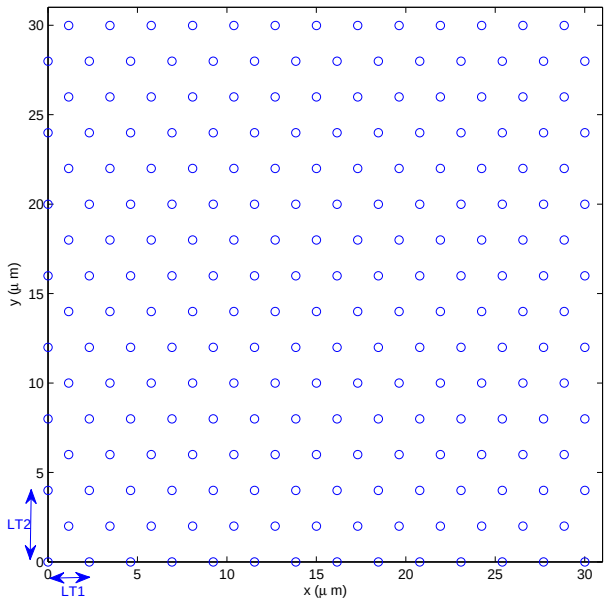

Figure 2.4: Hexagonal Sampling grid for T1 = 1.1543 and T2 = 2.

2.3 Detector Packing Density

The resolution is dependent on number of pixels for any module and in terms of pure sensor way we call it as a detector packing. we are interested in comparing both rectangular and hexagonal detector packing for unit density. This way the we compare both the processing performance can be a valid comparison. Sampling density is defined as number of samples per unit area. The rectangular packing is shown in Fig.5a and the hexagonal packing is shown in Fig.5b. The over all idea from

Fig 5 is to show that the Hexagonal packing is more efficient than the Rectangular packing with 13.4 % less sampling requires to achieve same density. From observing the Fig.5 it's clear that we can reduce aliasing by replacing the rectangular patter with hexagonal lattice.

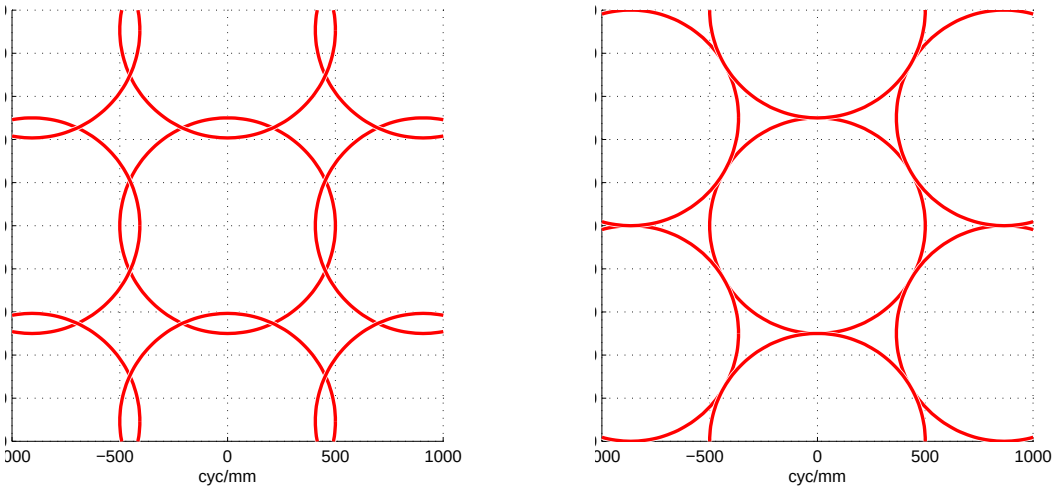

(a) (b)

Figure 2.5: Comparing Aliasing effect (a) CSFT of Rect when, $a = 1.1\mu m$, $\lambda = 0.5\mu m$, $f - number = 4$ showing 13.4% aliasing. (b) CSFT of Hexa when, $T1 = 1.15\mu m$, $T2 = 2\mu m$, $\lambda = 0.5\mu m$, $f - number = 4$ with no aliasing

2.4 Observed Image

Observed image is output from the observation model. We add noise to the sampled LR images to generate the observed image. With additive noise given by $g_i = f_i + n_i$, where n is an $N \times 1$ array of noise samples. Note that all of the LR pixel values can be combined into a single vector yielding $g = [g_1, g_2, ...g_N]^T$. On the other hand, the ideal HR image is obtained by sampling *d(x,y)*at the Nyquist rate, first the *d(x,y)* is band limited to ρ_c. Let this Ideal HR image is represented in lexicographical notation with the $N \times 1$ vector d as shown in Fig.1, Where N is total number of HR pixel. The image we wish to estimate from g is shown in Fig.1.

CHAPTER 3

HEXAGONAL TO RECTANGULAR RESAMPLING WITH ADAPTIVE WIENER FILTER

AWF is one SR method, which was mainly designed to work on multiple frame of Low Resolution (LR) images of the same scene to produce one HR image. AWF is tested within the current work for single frame. Within this work, there is only one LR image available as an input for the AWF.

We discuss an overview of the AWF algorithm presented originally in [2], and it is repeated here for readers convenience and it is shown in Fig. 3.1

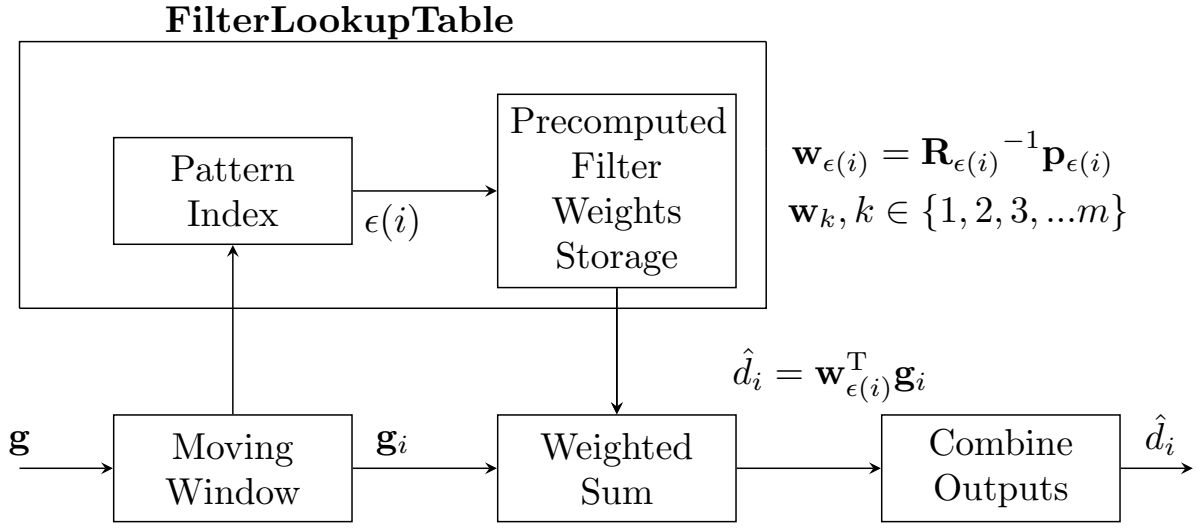

Figure 3.1: Single Frame AWF.

The AWF [2] is very use full in registering low resolution frames to a HR image

and it was proved my Dr. Russell Hardie in 2007. Later the filter is used for so many applicaions.

3.1 Single Frame AWF

An overview of the system is shown in Fig. 3.1. The AWF-SR algorithm uses a moving window that passes a over the HR grid of nonuniformly sampled data g. Let the samples in the small moving observation window about the ith HR output pixel be denoted $\mathbf{g}_i$. The output of the AWF is an estimate of the desired high resolution image and is giving by weighted sum for each HR pixel as follows.

$$\hat{d}_i = \mathbf{w}_{\epsilon(i)}^{\mathrm{T}} \mathbf{g}_i, \tag{3.1}$$

where $\mathbf{w}_{\epsilon(i)}$ is a vector of weights. Here $\epsilon(i)$ is a pattern index. The pixel are arranged in a hexagonal pattern and the sliding window search for different patterns, calculates the weight matrices and stores. if the same window of pixels appears then the algorithm reuses the store pattern weight values. The comparison of Ideal rectangular, HR and hexagonal grids are shown in Fig. 3.2.

The moving window is used to move across the LR image in steps of D_x and D_y in the horizontal and the vertical direction, respectively and it is of size W_x in the horizontal direction and W_y in the vertical direction, where $1 < D_x < W_x$ and $1 < D_y < W_y$. Each observation window contains a number of LR pixels. It can be expressed as

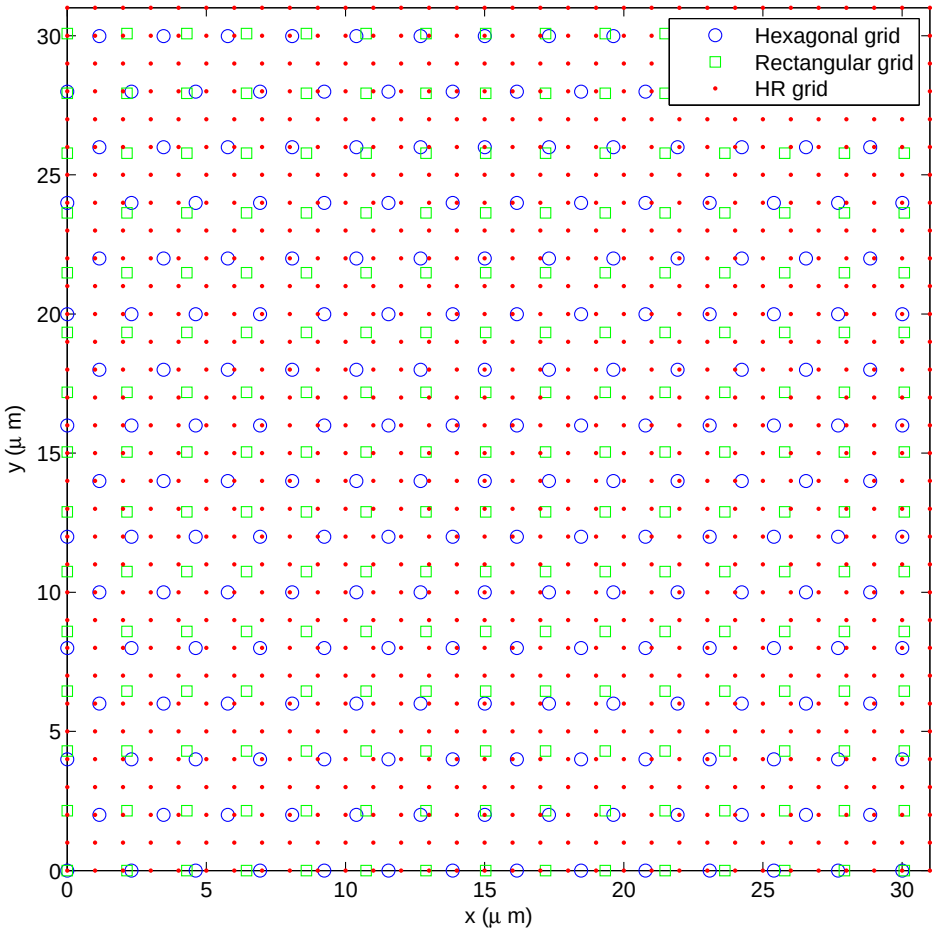

Figure 3.2: Comparison of Sampling grids showing the Ideal with $\bar{\Delta}_x = \bar{\Delta}_y = 1.0742\mu m$ and Hexa with $T1 = 1.1543$, $T2 = 2$ and Rect with $\Delta_x = \Delta_y = 1\mu m$.

$$k = \frac{W_x W_y}{L_x L_y}, \tag{3.2}$$

where L_x and L_y are the difference between the sampling rate of the estimated image and the sampling rate in the observation model in the horizontal and vertical directions, respectively. All the LR pixel are stored in the observation vector $\mathbf{g}_i$, where i is the index of the observation window locations. The LR pixel inside the observation

window are used in order to find an estimated pixel value $\hat{d}_i$ of the desired HR pixel d_i. The HR pixels are combined to compare with the desired HR image d.

Every group of $\hat{d}_i$ lie within the smaller subwindow inside the observation window called estimation window. Its size is D_x by D_y. A weighted sum is applied to the LR pixels such that

where $\hat{d}_i$ is a $D_x D_y \times 1$ matrix and $\mathbf{g}_i$ is a $K \times 1$ matrix. To be able to find the estimation of the HR pixels $\hat{d}_i$, the matrix $W_{\epsilon(i)}$ of size $D_x D_y \times K$, $\epsilon(i)$ is the pattern index show in filter look up table portion. The sliding window moves to a different set of pixel patterns and those are stored in the filter look up table for future use. The elements of $W_{\epsilon(i)}$ are found in a manner that minimize the mean square error between the observed image g and the desired image d so that

$$\mathbf{w}_{\epsilon(i)} = {\mathbf{R}_{\epsilon(i)}}^{-1} \mathbf{p}_{\epsilon(i)}, \tag{3.3}$$

where $\mathbf{R}_{\epsilon(i)} = E\{\mathbf{g}_i {\mathbf{g}_i}^T\}$ is the auto-correlation function of the observation vector, and $\mathbf{p}_{\epsilon(i)}= E\{\mathbf{g}_i {\mathbf{d}_i}^T\}$ is the cross correlation between the observation vector and the corresponding desire vector. Each column in the weights matrix is quantized, so that all of its elements would sum up to 1.

Now, both $\mathbf{R}_{\epsilon(i)}$ and $\mathbf{P}_{\epsilon(i)}$ need to be calculated, so that the weight matrix can be evaluated. To achieve that, let f_i be the observation vector without the noise. In other words,

$$f_i = \mathbf{g}_i + n_i, \tag{3.4}$$

where n_i represents the noise within the ith observation window. Assuming that the noise is independent with zero mean and has a variance of σ_n^2, then

$$\mathbf{R}_{\epsilon(i)} = E\{\mathbf{f}_i \mathbf{f}_i{}^T\} + \sigma_n^2 I, \tag{3.5}$$

and

$$\mathbf{P}_{\epsilon(i)} = E\{\mathbf{f}_i \mathbf{d}_i{}^T\}. \tag{3.6}$$

If the desired image has a wide sense stationary auto-correlation function $r_{dd}(x, y)$, the autocorrelation and the cross-correlation function of the noise free observation vector can be expressed as

$$r_{ff}(x, y) = r_{dd}(x, y) * h(x, y) * h(-x, -y), \tag{3.7}$$

and

$$r_{df}(x, y) = r_{dd}(x, y) * h(x, y), \tag{3.8}$$

respectively, where $h(x, y)$ is the PSF used to degrade the desired image $d(x, y)$ to get the noiseless observed image $f(x, y)$. When using the AWF algorithm the auto-correlations of the desired image can either be empirically obtained from training images, or it can be set as a parametric model. Most of the results included in AWF paper were obtained using a circularly symmetric parametric auto-correlation model.

$$r_{dd}(x, y) = \sigma_d^2 \rho \sqrt{x^2 + y^2}, \tag{3.9}$$

where σ_d^2 and ρ are acquired the matrices of the auto-correlation $\mathbf{R}_{\epsilon(i)}$ and cross-correlation $\mathbf{P}_{\epsilon(i)}$ can be found. Follow that, the weight matrices can be calculated, which will results the estimation of the HR pixel. The entire process of finding the weights and the estimated HR pixel is repeated for every observation window.

The auto-correlation model $r_{dd}(x, y)$ assumed above is a wide sense stationary. This does not apply to many images. To overcome this obstacle, the auto-correlation model should change according to the position of the observation window. This will make it affected by the change in the local intensity statistics of the samples. And the equation is shown below,

$$r_{dd}(x, y) = \sigma_{d_i}^2 \rho \sqrt{x^2 + y^2}. \tag{3.10}$$

$\sigma_{d_i}^2$ represents the variance of the local area in the desired image that corresponds to the ith observation vector.

Using $\sigma_{d_i}^2$ instead of σ_d^2 make the variance change with the position of the observation window. This implies that a $\sigma_{d_i}^2$ is measured for each observation window. The variance of the desired and degraded images are related as

$$\sigma_{d_i}^2 = \frac{1}{c(\rho)} \sigma_{f_i}^2, \tag{3.11}$$

where

$$c(\rho) = \int_{\infty}^{\infty} \int_{\infty}^{\infty} \rho^{\sqrt{x^2+y^2}} * h(x, y) * h(-x, -y) dx dy \tag{3.12}$$

Along this work, the noise is assumed to be independent. So, the variance of the

noise less observation vector can be obtained from the observation using the form

$$\sigma_{f_i}^2 = \sigma_{g_i}^2 - \sigma_n^2. \tag{3.13}$$

Now $\sigma_{f_i}^2$ is used to find $\sigma_{d_i}^2$. If the wide stationary auto-correlation model with a $\sigma_d^2 = 1$ was used, then

Changing the pixel dimensions of an image is called resampling [4]. Resampling also affects the display size of the image. Downsample, meaning that decrease the number of pixels in the image, information is deleted from the image. When we resample up, or increase the number of pixels in the image, new pixels are added based on color values of existing pixels. Resampling[5] can results in poor image quality. for example when we re sample an image to larger pixel dimensions, the image will lose some details and sharpness.

CHAPTER 4

RESULTS

In this section we present the experimental results that includes simulated data and the simulated data allows for quantitative performance analysis. we also examine and compared both sampling process.

4.1 Simulated Data on a Chirp Pattern

The chirp pattern has high frequency elements that are stacked together. The Fig. 4.1 shows a chirp pattern image that is processed with three different methods. Fig. 4.1(a) is an observed image. The HR image is degrade by different parameters and used as an input to all three methods. Fig. 4.1(b) is rect-griddata, processed, Fig. 4.1(c) is Hexa Griddata processed and Fig. 4.1(d) is AWF Hexa processed.

Hexa AWF processed image is look much closer to the observed image in terms of detecting high frequency lines.

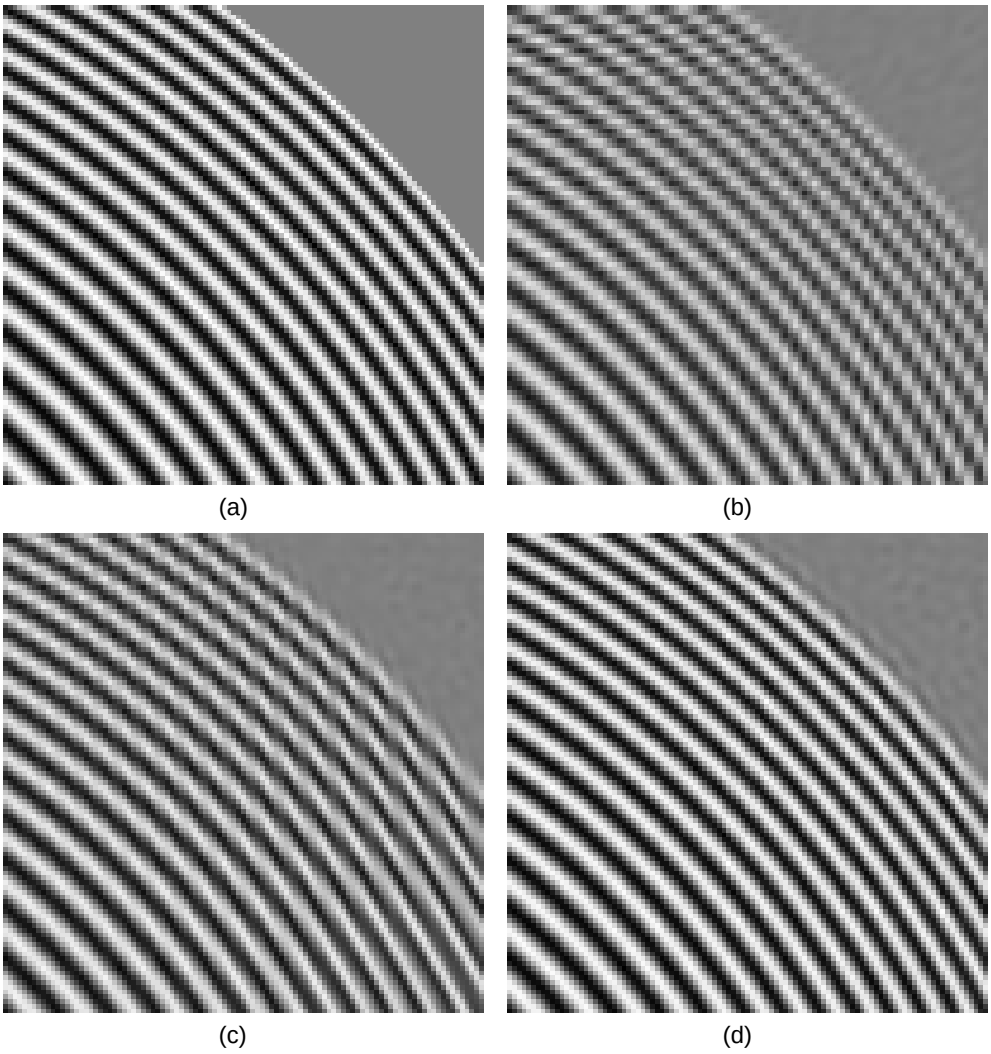

Figure 4.1: Chirp image (a) Observed image (b) Rect-griddata processed (c) Hex Griddata Processed (d) Hexa AWF processed .

4.2 Simulated Data on House Image

The house image is also a good example to see the aliasing issue. The Fig. 4.2 shows a house image that is processed with three different methods. Fig. 4.2(a) is

an observed image. The HR image is degrade by different parameters and used as an input to all three methods. Fig. 4.2(b) is rect-griddata, processed, Fig. 4.2(c) is Hexa Griddata processed and Fig. 4.2(d) is AWF Hexa processed.

Hexa AWF processed image is look much closer compared to the observed image in terms of detecting high frequency lines.

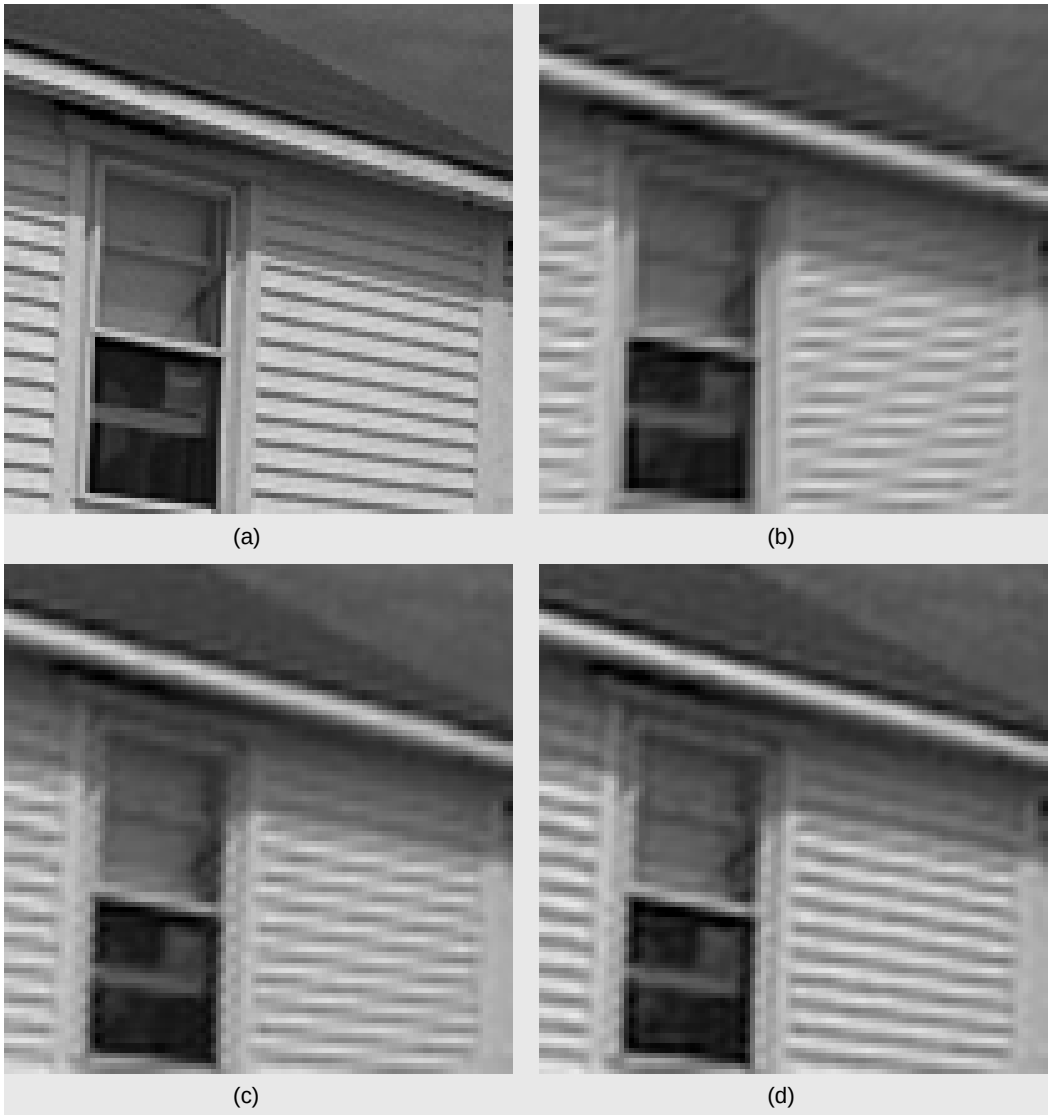

Figure 4.2: House image (a) Observed image (b) Rect-griddata processed (c) Hex Griddata Processed (d) Hexa AWF processed .

4.3 Simulated Data on Kodak Database- Boat Image

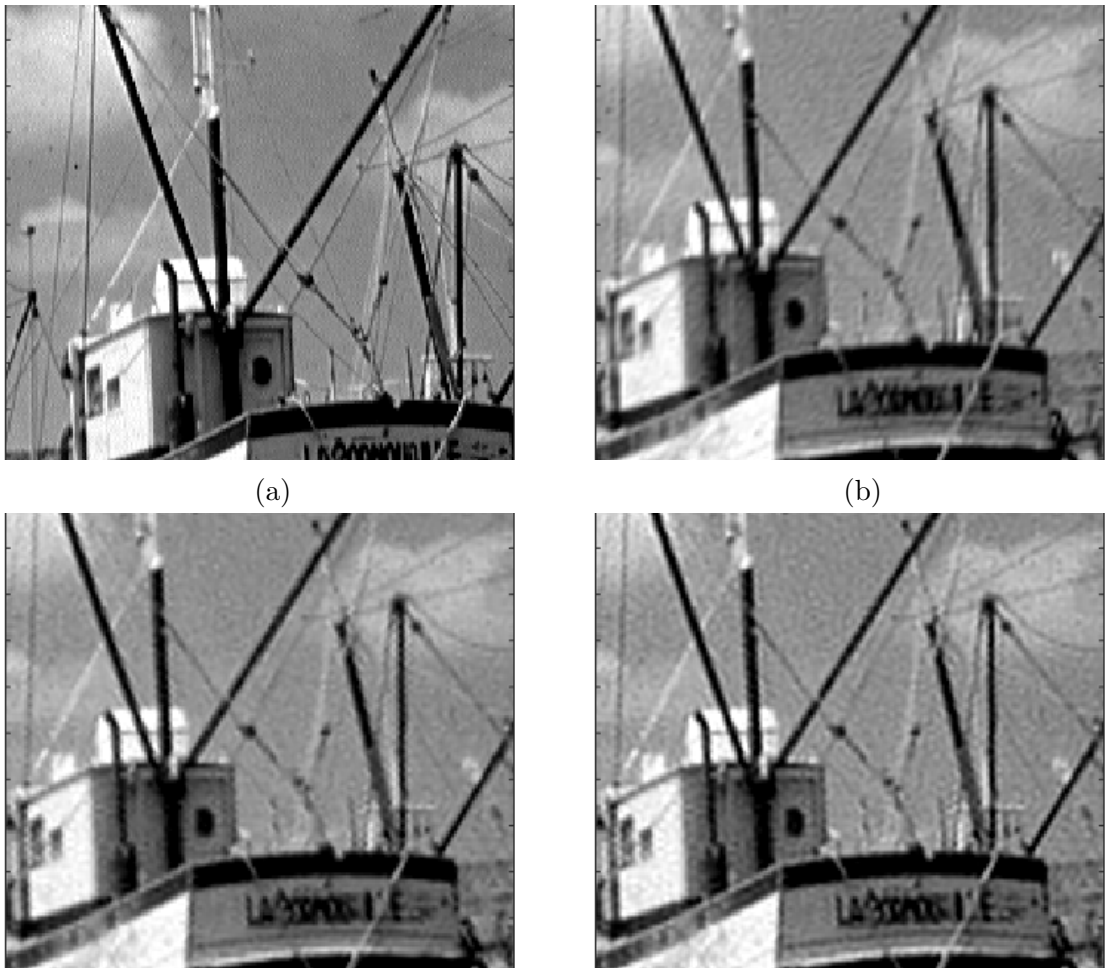

(a) (b)

(c) (d)

Figure 4.3: Comparing Noise level 2 std's and L2 (a)Observed Image (b) Rect Griddata Process, (d) Hexa griddata Process. (e) AWF Hexa.

4.4 Simulated Data on Kodak Database- Byke Image

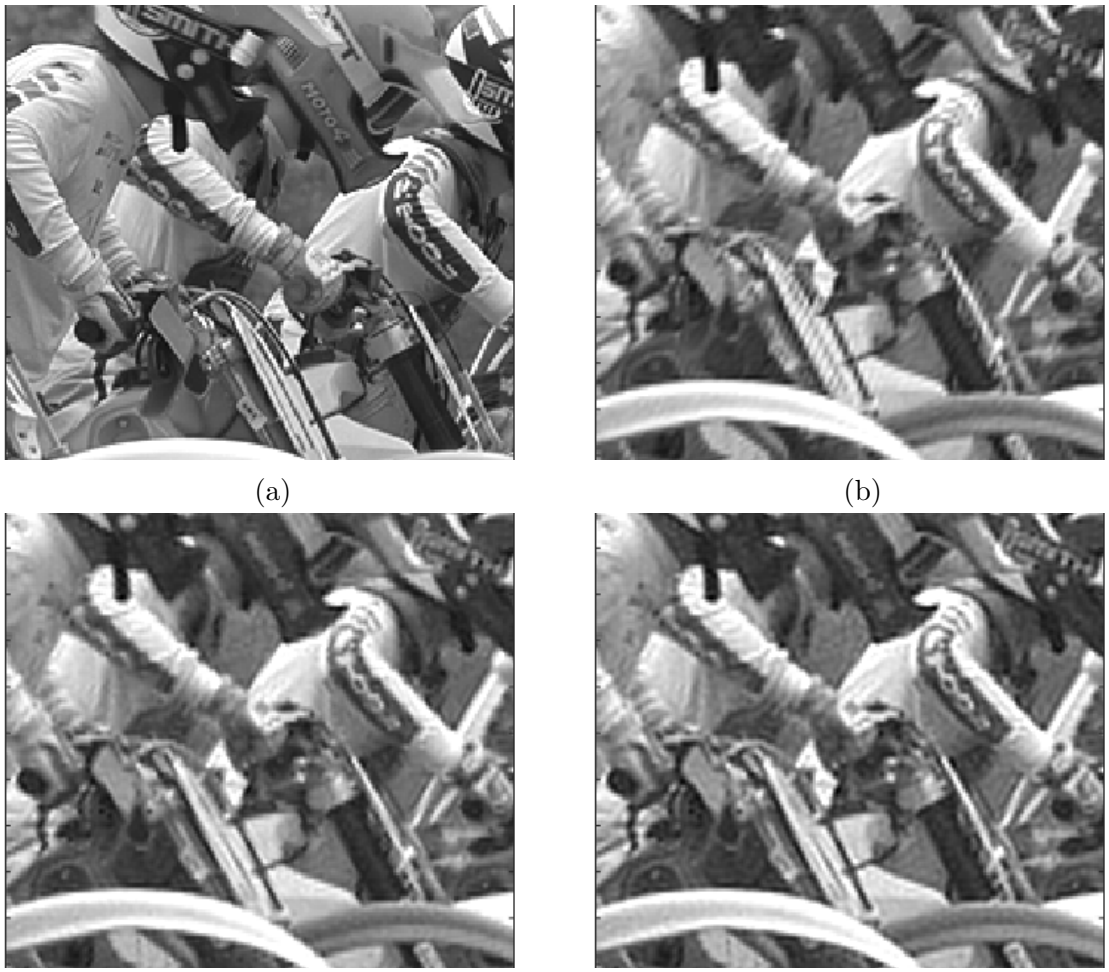

(a) (b)

(c) (d)

Figure 4.4: Comparing Noise level 2 std's and L2 (a)Observed Image (b) Rect Griddata Process, (d) Hexa griddata Process. (e) AWF Hexa.

4.5 Simulated Data on Kodak Database- House2 Image

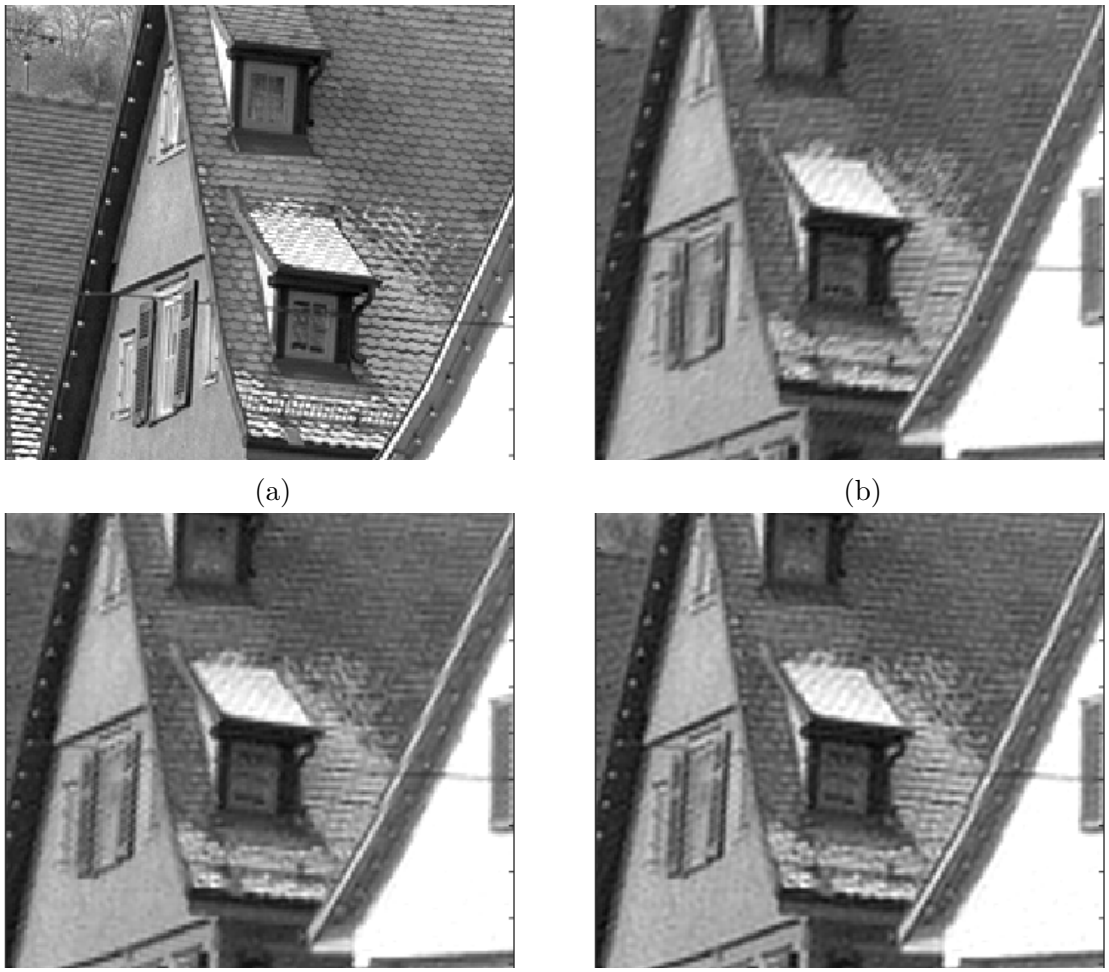

(a) (b)

(c) (d)

Figure 4.5: Comparing Noise level 2 std's and L2 (a)Observed Image (b) Rect Griddata Process, (d) Hexa griddata Process. (e) AWF Hexa.

4.6 PSNR Comparison of Simulated Data

PSNR comparision of Rect Griddata, Hexa Griddata and Hexa AWF are compared in Fig. 4.3. The over all performance of the Hexa AWF gave good results compared to other techniques for down sampling factor (L)is at 2 and 3.

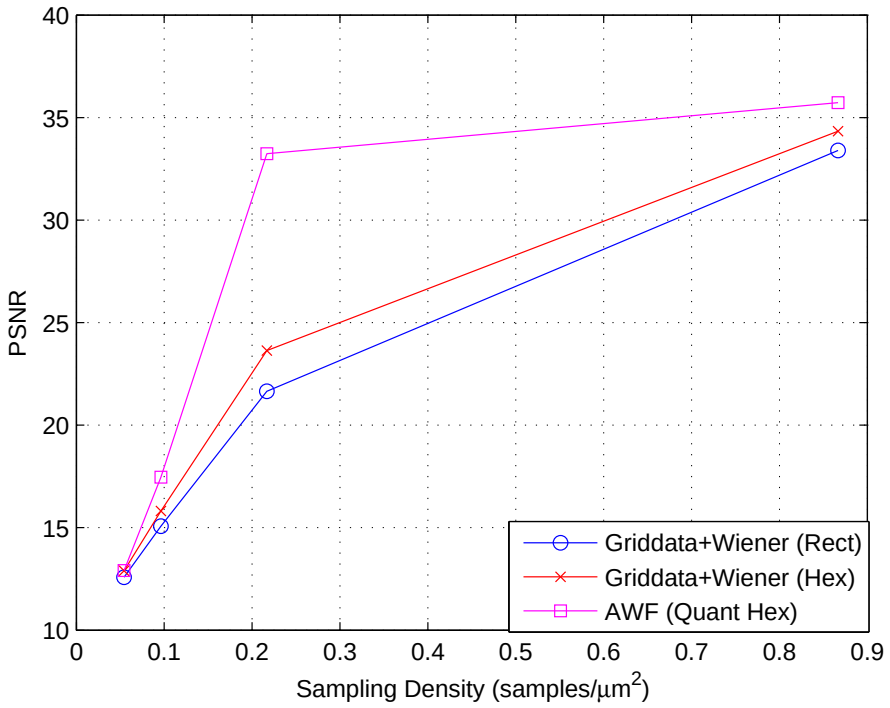

Figure 4.6: PSNR comparison of chirp image showing all three methods.

4.7 SSIM Comparison of Simulated Data

SSIM comparision of Rect Griddata, Hexa Griddata and Hexa AWF are compared in Fig. 4.3. The over all performance of the Hexa AWF gave good results compared to other techniques.

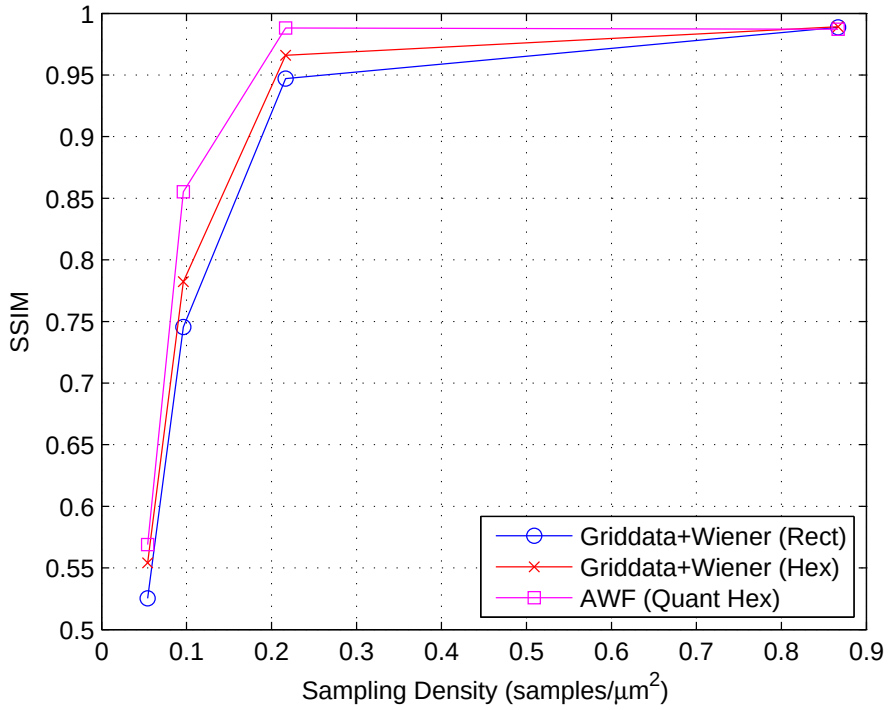

Figure 4.7: SSIM comparison of Chirp image showing all three methods.

4.8 PSNR and SSIM Results for Kodak Images

Table 4.1: Parameter Selected Values

Kodak image number	metric	Rect Griddata	Hex Griddata	AWF
1	PSNR	24.9650	25.5246	26.0043
	SSIM	0.7104	0.7450	0.7670
2	PSNR	31.8671	32.2996	32.5021
	SSIM	31.8671	32.2996	32.5021
3	PSNR	32.6276	33.2848	33.6057
	SSIM	0.8815	0.8908	0.8837
4	PSNR	31.9753	32.4667	32.9561
	SSIM	0.8509	0.8603	0.8641
5	PSNR	24.6720	25.2800	25.9160
	SSIM	0.7979	0.8215	0.8417
6	PSNR	26.5002	26.8387	27.2267
	SSIM	0.7536	0.7734	0.7904
7	PSNR	31.8538	32.3636	32.9986
	SSIM	0.9169	0.9220	0.9189
8	PSNR	22.5280	22.9343	23.5005
	SSIM	0.7433	0.7652	0.7861
9	PSNR	30.6660	31.2285	31.8794
	SSIM	0.8692	0.8774	0.8751
10	PSNR	31.0912	31.2594	31.6281
	SSIM	0.8718	0.8779	0.8770
11	PSNR	27.6901	28.1780	28.5661
	SSIM	0.7917	0.8088	0.8186

CHAPTER 5

CONCLUSION

We have proposed and tested re-sampling and restoration of hexagonally sampled image using AWF. The results obtained suggests that aliasing can be reduced by replacing the rectangular sampling scheme with the hexagonal sampling. Hexagonal structure is optimal and very useful in high end applications. The registration of non-uniform samples are accurately done with AWF and it's is proved that the AWF works for single frame registration also.

Tested kodak data base images and simulated data results are shown and the performance of the AWF hexa is dominant compared to all methods.

BIBLIOGRAPHY

[1] Marcel J. E. Golay. Hexagonal Parallel Pattern Transformations. C-18(8):733–740, August 1969.

[2] R. Hardie. A fast image super-resolution algorithm using an adaptive wiener filter. *IEEE Transactions on Image Processing*, 16(12):2953–2964, 2007.

[3] Xiangjian He and Wenjing Jia. Hexagonal structure for intelligent vision. In *Information and Communication Technologies, 2005. ICICT 2005. First International Conference on*, pages 52–64, Aug 2005.

[4] Innchyn Her and Chi-Tseng Yuan. Resampling on a pseudohexagonal grid. *CVGIP: Graph. Models Image Process.*, 56(4):336–347, July 1994.

[5] Qingtang Jiang. Fir filter banks for hexagonal data processing. *Image Processing, IEEE Transactions on*, 17(9):1512–1521, Sept 2008.

[6] R. Keys. Cubic convolution interpolation for digital image processing. *Acoustics, Speech and Signal Processing, IEEE Transactions on*, 29(6):1153–1160, Dec.

[7] E. Luczak and A. Rosenfeld. Distance on a hexagonal grid. *IEEE Transactions on Computers*, 25(5):532–533, 1976.

[8] R. M. Mersereau. The processing of hexagonally sampled two-dimensional signals. 67:930–949, 1979.

[9] Lee Middleton and Jayanthi Sivaswamy. Edge detection in a hexagonal-image processing framework. *Image and Vision Computing*, 19(14):1071 – 1081, 2001.

[10] Daniel P. Petersen and David Middleton. Sampling and reconstruction of wave-number-limited functions in n-dimensional euclidean spaces. *Information and Control*, 5(4):279 – 323, 1962.

[11] P. C. Cosman R. M. Gray and K. L. Oehler. in digital images and human vision, 1993.

[12] Wesley E. Snyder, Hairong Qi, and William Sander. A coordinate system for hexagonal pixels. In *PROC. SPIE! THE INTERNATIONAL SOCIETY FOR OPTICAL ENGINEERING*, pages 1–2. 1999, 1999.

[13] Richard C. Staunton and Neil Storey. A comparison between square and hexagonal sampling methods for pipeline image processing, 1990.

[14] Charles A. Wüthrich and Peter Stucki. An algorithmic comparison between square- and hexagonal-based grids. *CVGIP: Graphical Model and Image Processing*, 53(4):324–339, 1991.